NOVA SCHOOL OF SCIENCE & TECHNOLOGY

DEPARTAMENT OF MATERIALS SCIENCE

Catarina Cuba Martins Lourenço

BSc in Micro and Nanotechnologies Engineering

ZrO_2 Nanostructures on Anisotropic Alginate Scaffolds for Osteochondral Tissue Engineering

MASTER IN MICRO AND NANOTECHNOLOGY ENGINEERING

NOVA University Lisbon

september, 2023

DEPARTAMENT OF
MATERIALS SCIENCE

ZrO_2 Nanostructures on Anisotropic Alginate Scaffolds for Osteochondral Tissue engineering

Catarina Cuba Martins Lourenço

BSc in Micro and Nanotechnology Engineering

Advisor: Henrique Vazão de Almeida
Researcher at CENIMAT|i3N, NOVA University Lisbon

Co-advisor: Daniela Gomes
Assistant Professor, NOVA University Lisbon

Examination Committee:

Chair: Rui Igreja,
Full Professor, FCT-NOVA

Rapporteurs: João Carlos Silva,
PostDoc Researcher, IST

Adviser: Henrique Vazão de Almeida,
Researcher at CENIMAT|i3N, Nova University Lisbon

Co-adviser: Daniela Gomes,
Assistant Professor, NOVA University Lisbon

MASTER IN MICRO AND NANOTECHNOLOGY ENGINEERING

NOVA University Lisbon
september, 2023

ZrO_2 Nanostructures on Anisotropic Alginate Scaffolds for Osteochondral Tissue engineering

Para os meus pais.

ACKNOWLEDGMENTS

Primeiramente, gostaria de agradecer ao professor Rodrigo Martins, Pedro Barquinha e Hugo Águas, bem como a todos os professores que fizeram parte do meu percurso académico, por todas as aprendizagens transmitidas, e pelo acesso às instalações do CENIMAT|i3N, que cedeu todo o equipamento e meios necessários para que esta dissertação se realizasse.

Aos meus orientadores, Henrique e Daniela, agradeço por todo o apoio e confiança depositada e por toda a sabedoria que me transmitiram. Obrigada por nunca me terem posto sob pressão, e por todas as dicas e ajudas preciosas. Ao professor José Inácio, investigador no CEDOC, muito obrigada pela sua disponibilidade, simpatia e pela ajuda prestada.

Aos meus pais e avós, não há agradecimentos suficientes por todo o apoio, não só durante a dissertação, mas ao longo destes 5 anos. Obrigada por me ouvirem a refilar e por lidarem com o meu desespero em alguns momentos, e por me terem puxado para cima e ajudado a seguir em frente. Obrigada por sempre acreditarem em mim e nunca duvidarem das minhas capacidades e por me darem as ferramentas necessárias para terminar mais um capítulo.

Obrigada aos meus amigos de Micro e Nano, por me terem aturado durante estes nãos, pelos ZOOMs até às tantas a fazer trabalhos de grupo, pela partilha de apontamentos, mas, essencialmente, pelas noites de copos e jantaradas. Um obrigada especial à Bá, por ser a minha companheira desde o dia 1, por me aturar como ninguém e por me ouvir a queixar 24/7.

Um profundo obrigada aos amigos de longa data Madalena, Inês, Brites, Machadinho pela vossa paciência e apoio durante os períodos mais difíceis; e aos meus amigos de Ambiente, especialmente à Margarida, ao Tiago e ao Armando, por terem sido um pilar durante estes 5 anos. Por fim, obrigada ao João e ao Gui, que apesar de terem chegado mais tarde à minha vida, tornaram o último ano muito melhor e mais divertido.

Apesar de acreditar que o futuro traz coisas maravilhosas, foram 5 nãos de muitas memorias, maioritariamente boas, que vao deixar saudades infinitas. Obrigada FCT NOVA.

"If we knew what it was we were doing, it would not be called research, would it?"

Albert Einstein

ABSTRACT

The osteochondral tissue is a highly specialized tissue that involves the combination of cartilage and subchondral bone, whose mechanical properties are challenging to reproduce through artificial constructions. The different compositions and mechanical properties of bone and cartilage indicate the complexity of this tissue interface, making it challenging for the design and fabrication of tissue engineering scaffolds.

To transcend the limitations of conventional therapies, such as the insufficient self-healing capacity of cartilage, bioengineering has been dedicated for many years to researching innovative approaches to the treatment and regeneration of osteochondral tissue.

For this reason, zirconia nanoparticles were incorporated in an alginate hydrogel by two methods. Cell proliferation, viability and differentiation were assessed. Additionally, preliminary studies on the hydrogel's stability, morphology, degradation and mechanical properties were studied.

Study shows that the ZrO_2 nanoparticles were successfully synthetized, obtaining a monoclinic crystalline phase, with a nanosphere format. When incorporated with the alginate scaffold, the nanoparticles showed good adhesion to the construct and enhanced porosity, high swelling capacity but a decrease on the mechanical properties. Cellular test showed good results of viability tests after 7 days.

Keywords: alginate, hydrogel, zirconia nanoparticles, tissue engineering

RESUMO

O tecido osteocondral é um tecido altamente especializado que envolve a combinação de cartilagem e osso subcondral, cujas propriedades mecânicas são difíceis de reproduzir através de construções artificiais. As diferentes composições e propriedades mecânicas do osso e da cartilagem indicam a complexidade desta interface tecidular, tornando-a um desafio para a conceção e fabrico de estruturas de engenharia de tecidos.

Para ultrapassar as limitações das terapias convencionais, tais como a insuficiente capacidade de auto-cura da cartilagem, a bioengenharia tem-se dedicado à investigação de abordagens inovadoras para o tratamento e regeneração do tecido osteocondral.

Por este motivo, foram incorporadas nanopartículas de zirconia num hidrogel de alginato através de dois métodos. Foram avaliadas a proliferação, viabilidade e diferenciação celular. Adicionalmente, foram efetuados estudos preliminares sobre a estabilidade, morfologia, degradação e propriedades mecânicas do hidrogel.

Os resultados obtidos mostram que as nanopartículas de ZrO_2 foram sintetizadas com sucesso, obtendo-se uma fase cristalina monoclínica, com um formato de nanoesferas aglomeradas. Quando incorporadas nos scaffolds de alginato, as nanopartículas mostraram uma boa adesão ao mesmo e aumentaram a sua porosidade, obtendo também uma boa capacidade de inchamento, mas uma diminuição das propriedades mecânicas. Os testes celulares mostraram bons resultados de viabilidade celular após 7 dias.

Palavras chave: alginato, hidrogel, nanopartículas de zirconia, engenharia de tecidos.

CONTENTS

LIST OF FIGURES

List of Tables

ACRONYMS

3D	Three dimensional
AAD	Adipic acid dihydrazide
ALG	Alginate
$CaCl_2$	Calcium chloride
ECM	Extracellular matrix
EDC	(1-ethyl-3-(3-dimethylaminopropyl)carbodiimide hydrochloride)
EDS	Energy dispersive X-ray spectroscopy
FIB	Focus Ion Beam
GF	Growth factors
NaCl	Sodium chloride
NHS	N-hydroxysuccinimide
NPs	Nanoparticles
PBS	Phosphate Buffered Saline
PCL	Polycaprolactone
PEG	Polyethylene glyco
PLLA	Polylactic acid

SEM	Scanning electron microscopy
XRD	X-Ray diffraction

SYMBOLS

ρ	Density of ethanol.
^{o}C	Degree Celsius.

1

INTRODUCTION

1.1 Osteochondral Tissue Structure

Osteochondral tissue refers to the structure that is made up of both bone and cartilage tissues [1]. The tissue is found in areas of the body where bones articulate or move against each other, such as the knee, hip, and shoulder joints [2].

The structure of osteochondral tissue varies depending on the location in the body, but generally, it can be divided into two main components: the articular cartilage and the subchondral bone.

The articular cartilage is a layer of smooth, white, shiny, flexible and supportive tissue that covers the surface of bones in a joint. It is made up of chondrocytes (cartilage cells), extracellular matrix (ECM), and collagen fibers [3]–[5]. It provides a lubricated surface that is able to reduce friction. The articular cartilage has no blood vessels or nerves, which means that it is avascular and aneural. Instead, it receives its nutrients and oxygen through diffusion from the synovial fluid that surrounds it. This also means that it has a limited capacity for repair and regeneration when damaged [6].

The subchondral bone is a layer of bone that lies beneath the articular cartilage. It is made up of trabecular bone and cortical bone, and contains bone marrow, blood vessels, and nerves, which work together to provide nutrients and oxygen to the adjacent cartilage tissue. The subchondral bone provides support for the articular cartilage and helps to distribute forces across the joint [7]. Overall, the structure of osteochondral tissue is designed to provide cushioning and support for the joints, allowing them to move smoothly and without pain.

However, injury or disease can disrupt the structure of the tissue, leading to pain, inflammation, and reduced mobility.

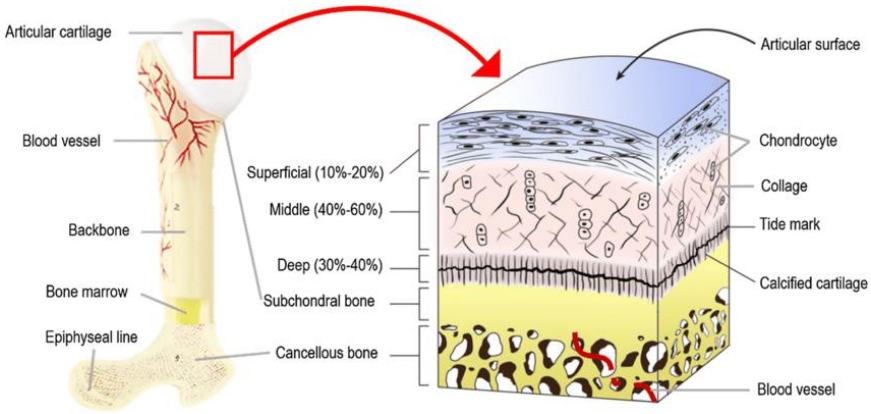

Figure 1. Histologic structure of a true osteochondral unit [8]

1.1.1 Osteochondral defects

Osteochondral and cartilage conditions are relatively frequent, particularly in elderly people and athletes [9] One of the most prevalent forms of osteochondral illness is osteoarthritis, a degenerative joint condition that can harm the bone and cartilage in joints. More than 32.5 million persons in the United States alone suffer with osteoarthritis, according to the Centers for Disease Control and Prevention (CDC) [10].

Rheumatoid arthritis, osteochondritis dissecans, and chondromalacia patella are more examples of osteochondral and cartilage illnesses. These disorders' prevalence can also change depending on elements including age, gender, and way of life [11].

1.1.2 Conventional therapies

The traditional methods of treating cartilage are palliative and reparative. In most cases, palliative strategies represent first-line treatment to reduce symptoms without addressing the causes [9]. The most common treatments for osteochondral defects are:

Non-surgical treatment: aims to reduce the pain and the inflammation of the joint by the use of medication such as ibuprofen, physical therapy, the use of protective wear or crutches, restriction of physical activity and immobilization [12], [13].

Surgical treatment: such as the removal of loose cartilage, microfacture, osteochondral allograft transplantation or stem cells injection [14].

Despite new therapies have been developed to treat osteochondral defects, articular cartilage and bone repair is still a major clinical challenge and still exist many shortcomings associated with these therapies, due to the insufficient self-healing capacity of cartilage and to the complexity of the osteochondral tissue [15].

1.2 Osteochondral Tissue Engineering

In order to overcome the use of conventional therapies, there is a critical need of exploring the field of tissue engineering as an alternative solution for bone and articular cartilage repair and regeneration. This therapeutic approach involves the use of cells, scaffolds, and growth factors (GF), trying to mimic the complex three-dimensional microenvironment of the joint that requires the interaction between these various components [9].

Tissue engineering is a multidisciplinary field of research conducted to meet clear clinical requirements of therapies to promote the regeneration and repair of diseased and damaged tissues [6]. Osteochondral tissue engineering is a field that aims to develop new strategies for repairing or replacing damaged or diseased cartilage and bone tissues. One of the main challenges in osteochondral tissue engineering is to recreate the complex structure and mechanical properties of natural cartilage and bone tissues [16], [17] .

1.2.1 Scaffolds

Scaffolds are one of the fundamental elements of tissue engineering approaches to osteochondral repair [18]. They support three-dimensional (3D) tissue development and they are made of biomaterials.

The ideal scaffold should have the following qualities to ensure the quality of tissue regeneration: should be biomimetic, mechanical properties that are compatible with the surrounding tissue, a porous structure for cell survival and material transport, an appropriate surface for cell adhesion, proliferation and differentiation, biocompatibility with minimal immunoreaction and bioabsorbability with a controlled rate of degradation [15][19]. After implantation, it should integrate into the lesion site and support the healing process.

Therefore, the design of biomaterials with sufficient mechanical qualities to promote subchondral bone regeneration, while preserving a relatively weaker structure allowing for cartilage repair, is at the core of the development of scaffolds [20].

1.3 Biomaterials

Biomaterials are the backbone of 3D engineered constructs and support tissue growth and formation by providing a similar environment to the native tissue and structural integrity throughout maturation to enable cell proliferation, cell-to-cell communication, and ECM (extracellular matrix) formation [21]. Biomaterial scaffolds can be produced from different

sources such as naturally derived polymers (such as chitosan, gelatin, collagen), synthetic polymers (like PEG, PCL, PLLA) and ceramics (hydroxyapatite, bioglass, biociments) [20].
Careful selection of appropriate biomaterial is an important aspect for tissue engineering research. The chosen biomaterial must be stable enough in aqueous media to tolerate handling, implantation, and, if necessary, mechanical stimulation, as well as offer an environment for cells that is similar to the natural ECM (biomimetics) [19].

1.3.1 Alginate

One biomaterial with particular interest is alginate, since it has outstanding properties in terms of biocompatibility, biodegradability, non-antigenicity, low toxicity, ease of gelation and low cost. Alginate is a naturally occurring anionic and hydrophilic polysaccharide. It is one of the most abundant biosynthesized materials and is derived primarily from brown seaweed and bacteria [21]. This negatively charged polymer has many applications such as food industry, drug delivery and tissue engineering.
Alginate is constructed of blocks of (1,4)-linked mannuronic acid (M) and guluronic acid (G) residues and is a linear copolymer, or a polymer built from more than one type of monomer. These residue blocks' composition, organization, and size are vital elements that affect how alginate behaves physically. [22].

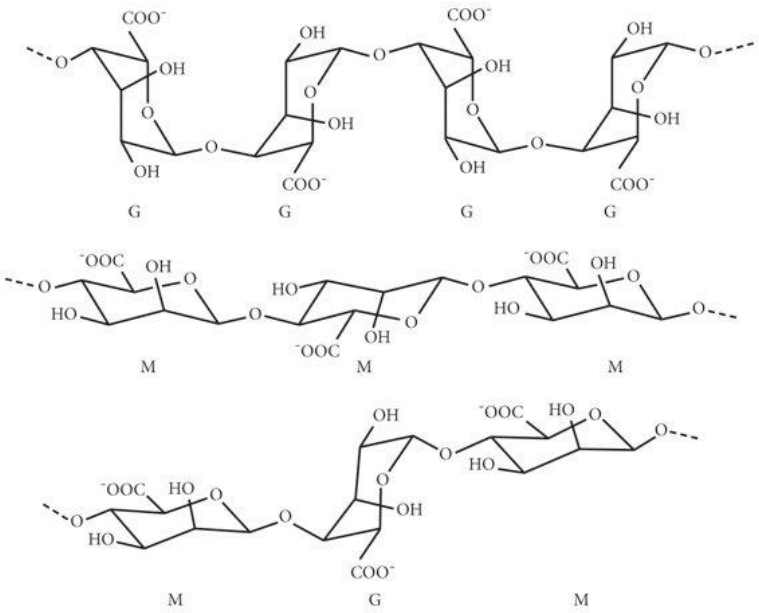

Figure 2. Representation of alginate structure [23].

1.4 Zirconia Nanoparticles

Zirconium dioxide, also known as Zirconia (ZrO_2), is a white crystalline oxide of zirconium. It is used in a variety of applications due to its characteristics such as high melting and boiling point, high resistance to chemical corrosion, high hardness and toughness, low thermal conductivity and it is biocompatible, making it a suitable material for medical applications [24]. Zirconia can exist in three crystalline states: monoclinic, - stable at <1150ºC- tetragonal- stable between 1150-2300 ºC- and cubic- stable at temperatures above 2300ºC [25].
Zirconia nanoparticles are small particles of the ceramic material zirconia ($Zr\mathit{O}_2$), which has a diameter of less than 100 nanometers.

1.4.1 Nanoparticle synthesis

Zirconium oxide nanoparticles (ZrO_2) can be synthesized by several techniques, such as sol/gel method, vapor phase method, pyrolysis, spray pyrolysis, hydrolysis, hydrothermal and microwave plasma [24], [25]. However, these methods faced many limitation factors such as complicated procedures, high reaction temperature, long reaction time, toxic reagents and by-products use, and high cost of production, which made it difficult to prepare zirconia nanoparticles on a large-scale production.
Considering the materials' sustainability, green solution synthesis techniques can be used like microwave hydrothermal synthesis. Microwave hydrothermal synthesis is a method used for the creation of nanoparticles at high pressures and temperatures. It creates nanoparticles quickly and effectively by combining hydrothermal synthesis and microwave heating. It utilizes microwave radiation to generate heat within the reaction mixture directly. The microwaves rapidly and uniformly heat the reaction vessel, leading to faster reaction rates and reduced synthesis times compared to conventional methods. This technique takes advantage of the selective absorption of microwaves by polar molecules, such as water, which significantly accelerates the hydrothermal reaction [26].
This technique can synthesize nanoparticles with a narrow particle size distribution and uniform morphology, despite being fast and simple and using water as solvent. Another important aspect is that this technique is compatible with several eco-friendly substrates, including cellulose-based ones [26].
Therefore, in this thesis, hydrothermal synthesis using microwave was chosen to produce Zirconia nanoparticles, followed by a calcination process.

2

MATERIALS AND METHODS

2.1 Alginate Scaffolds Production

2.1.1 Alginate Solution

The alginate solution was adapted based on previously published work from Vazão de Almeida et al [27]. The obtained hydrogel was transferred to a Petri dish and gelified overnight. Then, it was washed with deionized water and 0.1M of $CaCl_2$ to remove chemical agents. More information can me found in the Appendix A1.

2.2 Characterization Techniques of the Scaffolds

SEM Analysis: The morphology of scaffolds was investigated using SEM in Hitachi S-2400 equipment, with an accelerating voltage set to 15 kV.

Mechanical Analysis: Compression tests were performed using 3 scaffolds of each group using a tensile equipment (MINIMAT firmware v3.1) at room temperature, with a load cell of 20 N. The load was applied to the sample at a speed of 1 mm/min. This mechanical analysis was performed to wet samples.

Porosity: The scaffolds were immersed in ethanol for 5 minutes and the samples were weighted before (W_1) and after (W_2) the immersion. The calculation of the porosity uses the following formula [28]:

$$Porosity\ (\%) = \frac{W_2 - W_1}{pV_1} \times 100$$

Where V_1 indicates the volume before immersion and p is the density of ethanol.

Swelling Ratio and Degradation Studies: The gravimetric method was used to assess the scaffolds' water absorption capabilities. To achieve equilibrium swelling, the freeze-dried hydro-

gels (W_0) were incubated in 1 mL each of PBS for 2 days, at 37 °C. The weight of the hydrogel after swelling (W_S) was calculated, using the following formula [29]:

$$SR\ (\%) = \frac{W_S - W_O}{W_O} \times 100$$

All measurements were executed in triplicate.

Similarly, biodegradation assessment was carried out by immersing the scaffolds in PBS and monitoring the weight loss. Mass degradation was tested at various periods up to 14 days. The remaining hydrogel was calculated using the formula [29]:

$$W\ (\%) = 100 - \left(\frac{W_0 - W_f}{W_0} \times 100\right)$$

Where W_f is the dry weight of sample after degradation and W_0 is the initial dry weight of the sample.

Live/Dead Staining: The viability of the cells and their morphological changes were assessed on days 1 and 7. The images were captured using a Zeiss Axiovert 40 CFL microscope. The cytotoxicity of the cells was also evaluated.

2.3 ZrO_2 Nanoparticles Production

The oxide zirconium nanoparticles were synthesized via hydrothermal synthesis assisted by MARS microwave. The nanoparticles synthesis route was adapted on previously published work [27].

After microwave synthesis, the dried ZrO_2 nanopowder was further calcinated in an alumina ceramic crucible at 800 °C for 1 hour using a Nabertherm furnace under atmospheric conditions, in order to achieve the formation of the monoclinic phase- the most thermodynamically stable one.

2.4 Characterization Techniques of ZrO_2 NPs

XRD Measurements: XRD experiments were carried out using a PANalytical's X'Pert PRO MPD diffractometer (Almelo, The Netherlands) equipped with an X'Celerator 1D detector and using CuK_ radiation (λ =1.540598 Å). XRD data were recorded from 20° to 80° 2Θ range with a step of 0.05°.

SEM Analysis: The surface morphology of ZrO_2 nanoparticles was analysed by scanning electron microscopy (SEM) combined with a focused ion beam (FIB) workstation (Carl Zeiss AURIGA Microscopy GmbH, Oberkochen, Germany).

Raman Spectroscopy: Raman spectras were obtained using Raman spectroscopy (inVia Qontor confocal Raman microscope from Renishaw (Kingswood, UK)). The excitation source used was a 50 mW green diode operating at 532 nm, with an exposure time of 10 s. The Raman spectra were recorded in the range of 110–800 cm^{-1} (as an extended scan).

2.5 Scaffold with ZrO_2 Ps

Two methods were tested in order to incorporate zirconia nanoparticles with the alginate scaffold: a soaking method- where the freeze-dried scaffolds were soaked in zirconia nanoparticle solution – and a blending method- the alginate solution was mixed with the zirconia nanopowder before lyophilization. In each one, three percentages of ZrO_2 nanoparticles were evaluated: 0.25%; 1.0% and 1.5%.

Soaking Method: A solution of 2 mg of PEG 35000 (Sigma-Aldrich, CAS: 25322-68-3) was dissolved in 10 mL of deionized water and kept in agitation for 24 hours. Simultaneously, 0.25% w/v ZrO_2 NPs was dispersed in 3 mL of distilled water in an ultrasound bath for 30 minutes, at room temperature. Finally, 1.8 mL of the first solution was mixed with 3 mL of the solution containing the nanoparticles and kept in agitation for 6 hours at 50ºC. This procedure was repeated for the solutions containing 1% and 1.5% of ZrO_2 NPs. Then, the freeze-dried alginate scaffolds were immersed in 50 microliters of the final solution.

Blending Method: The protocol used before to produce alginate scaffolds was adapted in order to obtain an ALG/ ZrO_2 nanoparticles solution. After adding the sodium alginate in the solution containing MES and NaCl, the nanoparticles were added in different concentrations. After that, the whole procedure was identical to the one described by Henrique V. Almeida[27], that can be found in Appendix A.1.

3

RESULTS AND DISCUSSION

3.1 Morphological and structural characterization of Zirconia Nanoparticles

Figure 3 shows the SEM Images of ZrO_2 NPs synthesized under microwave irradiation followed by a calcination treatment at 800°C for 1 hour. The synthesized nanoparticles are displayed in the form of aggregated nanospheres. The particles have been measured using ImageJ software. In appendix can be seen a representation of measures taken from Figure 3, where 20 random particles were used. The average diameter of the measured NPs is 66.19 ± 7.55 nm.

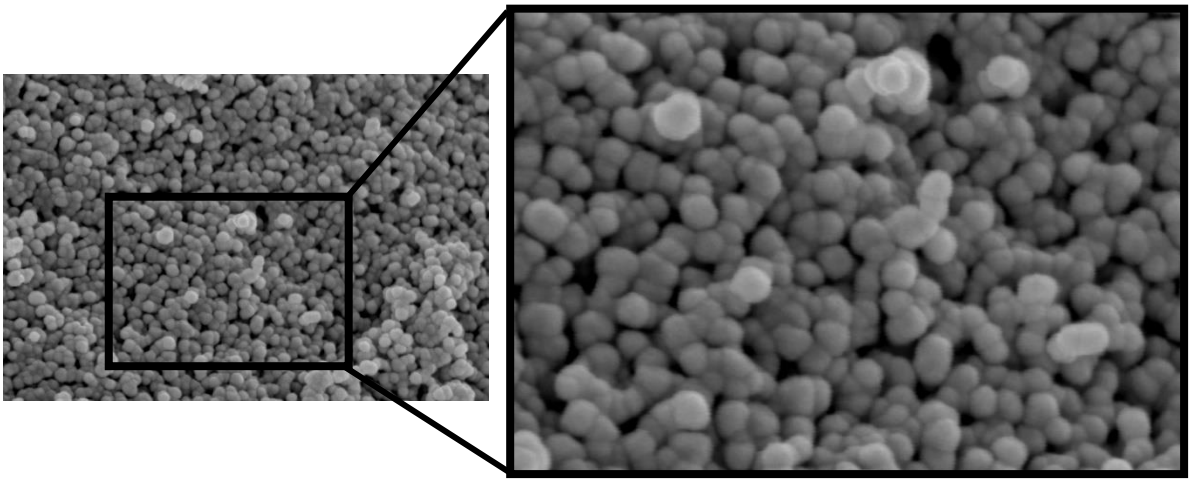

Figura 3. SEM image of synthetized ZrO_2 nanoparticles.

To confirm the crystalline phase present in ZrO_2 nanoparticles, both XRD and Raman techniques were performed. To identify the phases present in a sample, the obtained results should be compared with a database containing known diffractograms. In the specific case of this study, the reference codes used for data interpretation were ICDD 00-036-0420 (for

monoclinic phase), ICDD 00-050-1089 (for tetragonal phase) and 00-051-1149 (for cubic phase).

As we can observe in Figure 4 a)., the characteristic peaks of monoclinic ZrO_2 are present: (011) at 2 θ =24.0, (-111) at 2 θ =28.2, (111) at 2 θ =31.4, (002) at 2 θ =34.1, (022) at 2 θ =49.2 and (-220) at 2 θ =50.1. These are in agreement with the cards from literature that can be found in the Appendix A.3 (m- ZrO_2, JCPDS cards no. 00-036-0420). It is important to notice that peaks at 2 θ =35.2 and at 2 θ =50.5 can belong to both the tetragonal phase (t- ZrO_2) or monoclinic phase (m- ZrO_2).

Therefore, both monoclinic and tetragonal phases can be present, considering the ICDD card numbers 00-036-0420 and 00-050-1089 for the ZrO_2 monoclinic and tetragonal phases, respectively. The cubic phase of zirconia nanoparticles was not found in this sample.

Since monoclinic and tetragonal phase can both be present in this nanoparticle powder, Raman technique was performed in order to understand if the nanoparticle powder is a mixture of monoclinic and tetragonal phases or just pure monoclinic phase. In Appendix A.3 the diffractograms of the crystalline phases of zirconia can be seen.

According to the literature [30]–[33], the Raman spectra of monoclinic zirconia is expected to present peaks at: 179 cm^{-1} (A_g), 190 cm^{-1} (A_g), 224 cm^{-1} (B_g), 305 cm^{-1} (A_g), 334 cm^{-1} (B_g), 348 cm^{-1} (A_g), 381 cm^{-1} (B_g), 476 cm^{-1} (A_g), 505 cm^{-1} (B_g), 536 cm^{-1} (B_g), 556 cm^{-1} (A_g), 616 cm^{-1} (B_g), 637 cm^{-1} (A_g). All the active vibrational modes in the spectra of Figure 4 b)., correspond to the monoclinic phase of zirconia. No additional peaks corresponding to any other phase were observed in Raman spectra of this sample.

Therefore, the synthesis performed to zirconia nanoparticles ensured a purely monoclinic phase of ZrO_2 NPs. Both peaks that could belong to tetragonal and monoclinic phases in the XRD analysis, correspond to the monoclinic phase, in this sample.

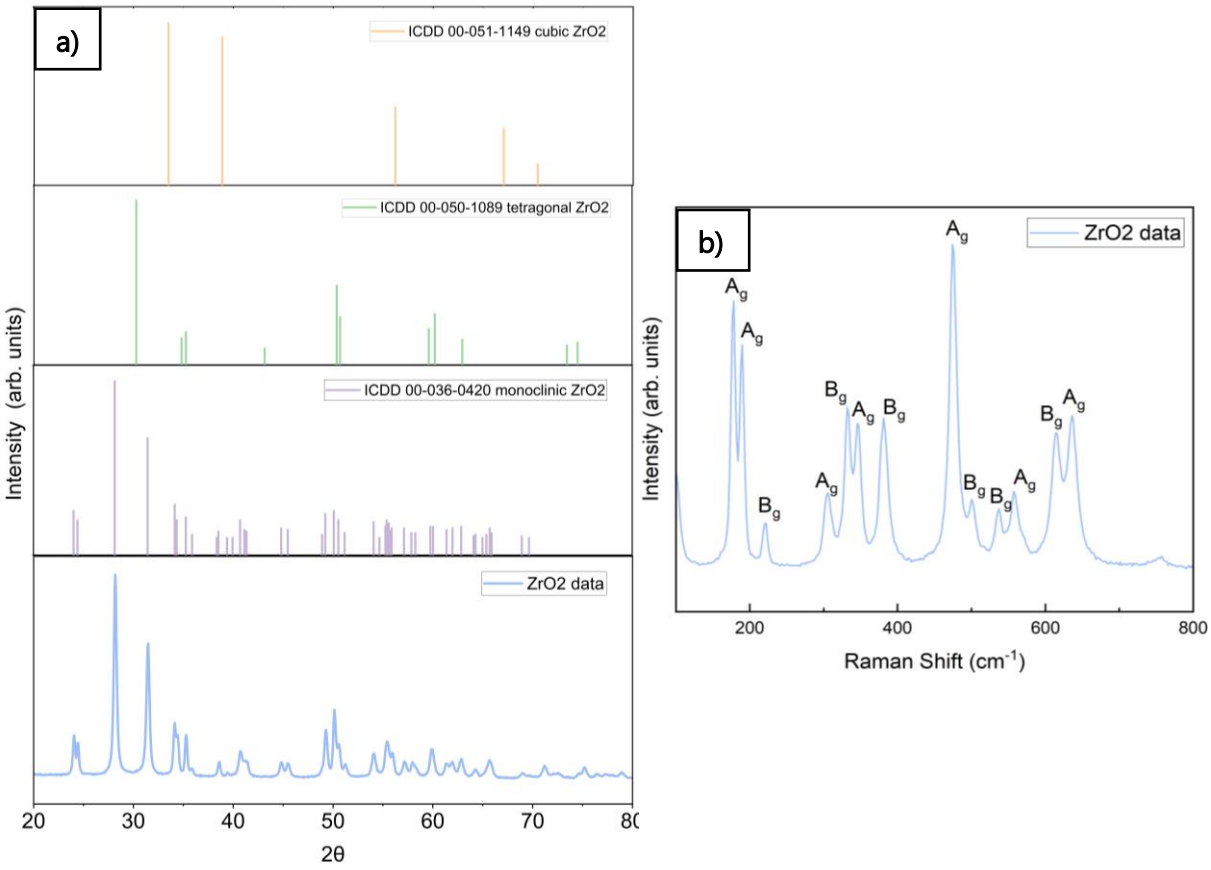

Figure 4. a) XRD diffractogram of ZrO_2 powder produced by microwave synthesis. For comparison, the simulated monoclinic, tetragonal and cubic zirconia structures are also presented. b) Raman Spectra of ZrO_2 nanopowder.

3.2 Scaffolds Assessment

Seven scaffolds with different compositions, as described in section 2.5, were studied. The groups are denominated Control (just ALG), S025, S1, S15, B025, B1, B15, according to the concentration of zirconia nanoparticles: 0.25%, 1% and 1.5%, respectively. The S corresponds to the scaffolds incorporated by the soaking method and the B to the ones incorporated with the blending one.

3.3 Physical properties of the Scaffolds

In order to evaluate the physical properties of the scaffolds with different percentages of zirconia nanoparticles, SEM analysis, swelling, degradation, porosity and mechanical tests were made.

The morphology of the scaffolds from all ZrO_2 compositions was observed by SEM (Figure 5). It is possible to observe that both the soaking and the blending method of incorporating nanoparticles with the alginate generate two completely different types of images.

It is possible to observe that the surfaces of the scaffolds have been effectively covered with ZrO_2 NPs by the soaking method (Figure5 d), e), f)). The zirconia NPs seem to be spread over the entire surface, despite of some agglomerates. The adhesion of the NPs to the alginate surface by the soaking method was possible due to the freeze drying (also called lyophilization) technique. Also, the amount of nanoparticles present at the surface in the soaked scaffolds, causes a rough surface.

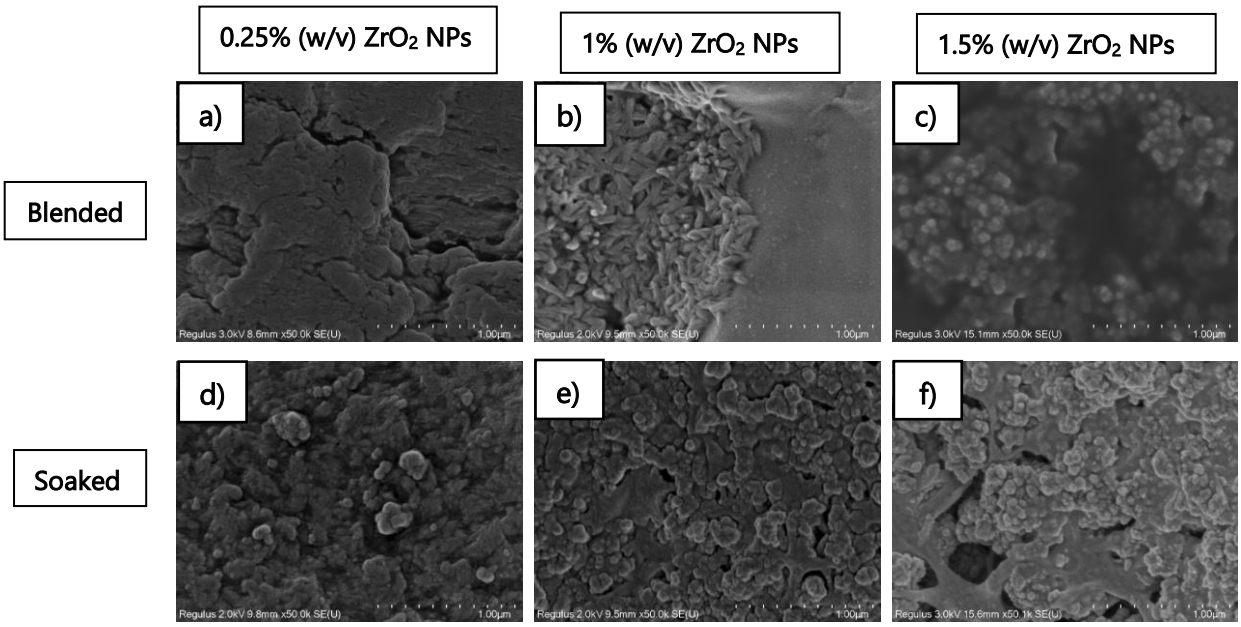

Figure 5. SEM images of blended and soaked scaffolds with different ZrO_2 percentages. a) blended with 0.25% NPs. b) blended with 1% NPs. c) blended with 1.5% NPs. d) soaked with 0.25% NPs. e) soaked with 1% NPs. f) soaked with 1.5% NPs. Scale bar: 1µm.

By the blending method, there is a bigger quantity of nanoparticles trapped inside the alginate, so the nanoparticles spheres are not so visible at the surface. 1B sample presents an accumulation of a substance, that could be NaCl, meaning that the dissolution time was not enough to the homogeneity of the reagents. In the case of the 15B sample, the image is hard

to analyse due to some impurities in the surface of the sample, but we can observe an increase of nanoparticles in the surface comparing with 025B and 1B.

The different incorporation of nanoparticles have different impact on the scaffolds morphology: by the blending method, it possible to obtain scaffolds with nanoparticles trapped in the scaffolds' matrix. On the other hand, the scaffolds produced by the soaking method obtain a greater quantity of nanoparticles attached to the surface.

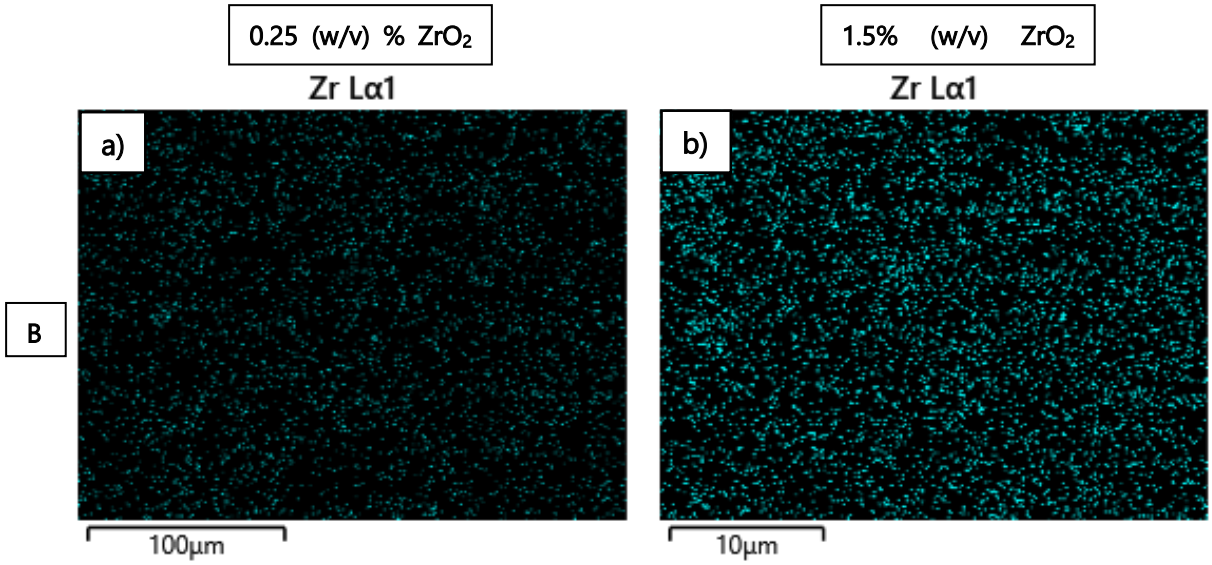

Figure 6. EDS analysis of two blended scaffolds. The corresponding EDS maps for Zr is presented. a) 025B. B)15B. Scale bar: a) 100 µm and b)10 µm.

The EDS technique was carried out in two samples to analyse the distribution of the nanoparticles and if they were spread in all alginate surface. It is possible to observe that the ZrO_2 nanoparticles are distributed all over the alginate surface, without having aglomarates in specific zones. It is also possible to check that the 15B sample has much more green dots- that correspond to zirconia NPs presence- than the 025B sample, as it was expected.

3.3.1 Porosity

The porosity of the scaffolds was calculated as described in the Experimental Procedure chapter. The pore fraction of a scaffold must not be too high to compromise the scaffolds' mechanical strength or too low to prevent cell migration, in order for the scaffold to function as a temporary bone tissue replacement element [34], [35].

As we can observe from Figure 7 and Table 1, the incorporation of ZrO_2 NPs by both methods decreases the porosity of the scaffold. Observing the values obtained, it is possible to conclude that with the rise of zirconia percentage, the porosity decreases.

Comparing both methods, the soaking one presents lower values of porosity, as we can confirm by Table 1 or Figure 7. This might be due to the fact that ZrO_2 nanoparticles were successfully incorporated into the surface, leaving less pores available for the absorption of ethanol. Therefore, the more nanoparticles percentage, the lower the porosity of the scaffold. On the other hand, the blending method presents higher values of porosity meaning that the nanoparticles are entrapped in the alginate and not so much at the surface, leaving more available porous to ethanol absorption.

The only value lower than the control group [24-39%] is the 15S, so we can infer that the addiction of nanoparticles increases the porosity of the alginate scaffolds.

In order to mimic the body's environment, the scaffolds must provide characteristics as similar as possible to those of the body. The scaffold should closely imitate the porosity found in adult human bone, where the outer cortical bone exhibits a porosity of 5-10%, and the inner cancellous bone displays a porosity of 75-85% [36]. From Table 1, the values of the trabecular bone can be mimic by 1B scaffold. 025B and 15B can also be considered due to the big standard deviation. 15S scaffold has a medium porosity value of 20.77% and, although it is higher, it is the closest value to mimicking the porosity of the cortical bone.

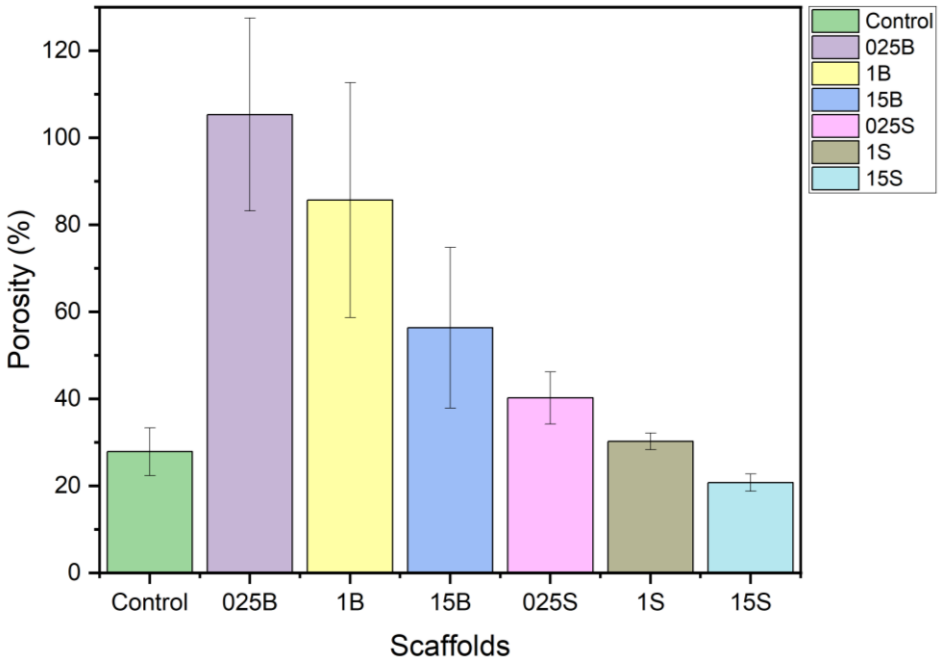

Figure 7. Porosity of the scaffolds.

Table 1. Scaffolds porosity and stand. deviation.

	Scaffolds	Porosity (%)
Control	ALG	31.06 ± 5.74
Blending group	0.25% of ZrO_2 NPs	105.35 ± 22.17
	1% of ZrO_2 NPs	85.66 ± 26.97
	1.5% of ZrO_2 NPs	56.32 ± 18.46
Soaking group	0.25% of ZrO_2 NPs	40.21 ± 6.01
	1% of ZrO_2 NPs	30.22 ± 1.90
	1.5% of ZrO_2 NPs	20.77 ± 2.00
Bone	Trabecular	75-90 [37]
	Cortical	5-10 [37]

When using a scaffold for tissue engineering, it is important to evaluate parameters like degradation and swelling rate, to assure that the structure survive and maintain its integrity over the cell culture period- 14 days. For that reason, swelling and degradation tests were performed submerging the scaffolds in an aqueous saline medium (PBS).

Figure 8 a). shows the evolution of scaffold swelling over the two-day period, expressed as a percentage of weight in relation to the dry measure, for the three types of samples analysed. From the trend of the curves and the values, it appears that the samples show increasing swelling, especially after 24 hours. After that, the values of all groups stabilized, as expected, since they reach their swelling capacity [37].

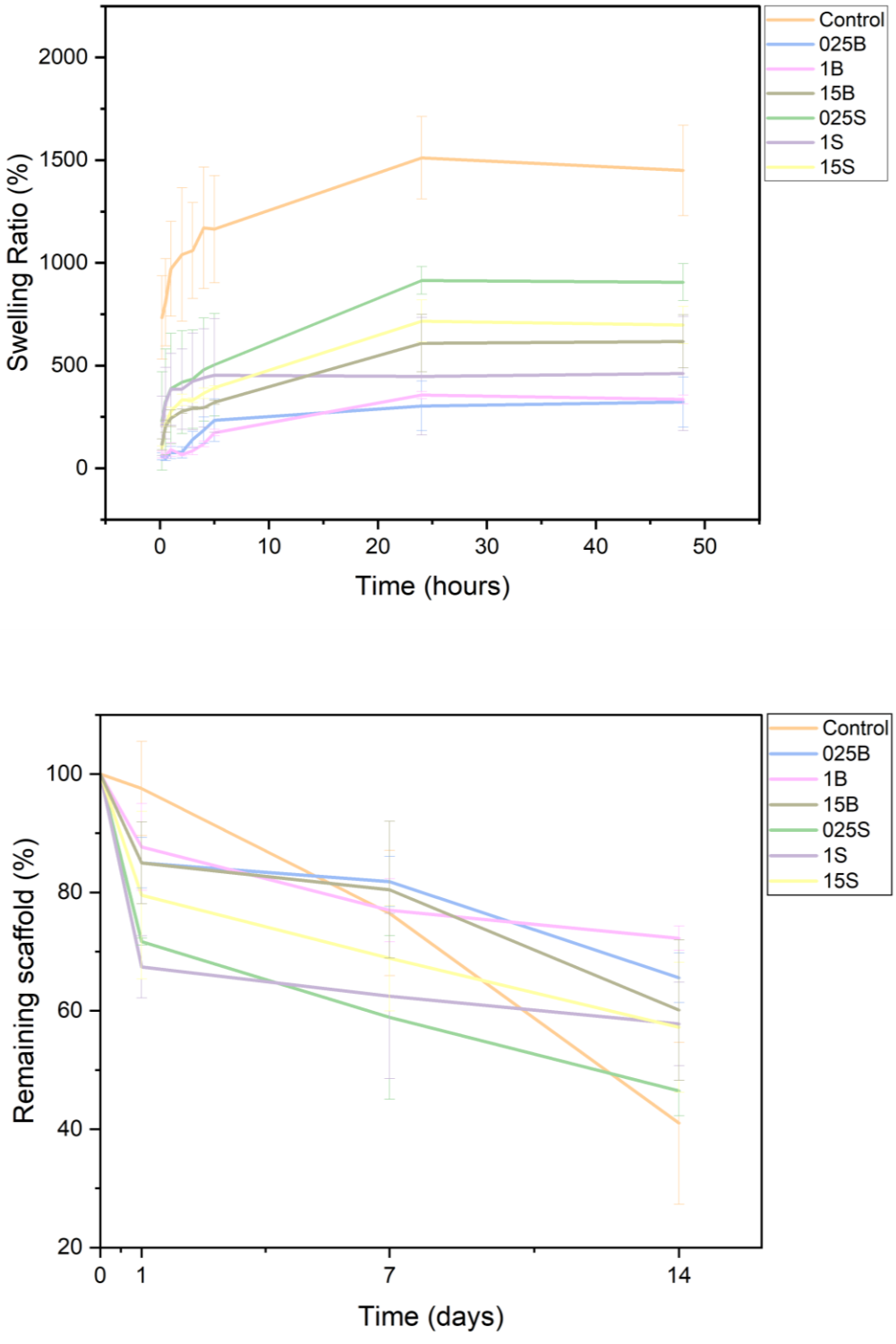

Figure 8. a) Swelling ratio of the scaffolds. b) Degradation rate of the scaffolds.

a)

The soaking groups present a very high swelling capacity, when compared to the blending ones. By the blending method, the scaffolds swelling capacity decreases with the addiction of nanoparticles. However, the behaviour of the scaffolds made by the blending method does not follow that logic, and the scaffold with the big amount of nanoparticles has the biggest swelling ratio. The hydrogel without reinforcement possesses the highest swelling degree. This is expected since the hydrogel system's tendency to swell normally reduces, with the addition of NPs [38]. The inclusion of the particles may encourage physical cross-linking of the structure, which would lessen swelling, depending on how they interact with the alginate molecular chains and their concentration. Additionally, less space will be available for water retention due to the presence of the nanoparticles inside the porous structure. Therefore, we can say that the nanoparticles decrease the swelling capacity of the biomaterial [29], [39].

All scaffolds in this study had good swelling ability because sodium alginate is a hydrophilic natural polymer material [23].

Since a higher porous structure of tissue engineering scaffolds provides higher water uptake, it was expected that the samples produced by the blending method had the biggest swelling ratio. This reverse situation, might be due to the fact that the concentrations of the nanoparticles used in this study are low, not influencing the swelling behaviour.

The degradation behaviour of the constructs over 14 days can be observed in Figure 8 b).

The weight loss in control group approached 59%, the weight loss in blended groups reached values between [28-40] % and the weight loss in the soaking groups approached values between [42-54] %, at the end of 14 days. As in swelling, the highest weight loss percentage was observed in ALG. The first reason is the swelling capacity for this situation. Control group had the higher swelling capacity than the groups functionalized with the zirconia nanoparticles. The samples' swelling ability causes more freedom for amorphous chains to move easily. As a result, even when crosslinked, ALG chains have a tendency to degrade rapidly during degradation tests because of their high swelling capacity.

After 1 day, the groups with the faster degradation rate were the ones made by the soaking method. This could be due to a weak attachment of the nanoparticles' solution used on the soaking method, that lead to its dissolution on the medium on the first day.

Comparing to other studies, the control group showed a degradation rate slower than expected [40]–[42]. This might be due to the effect of the crosslinkers, EDC, NHS and AAD, that provide a longer integrity to the scaffold.

3.3.2 Mechanical analysis

An example of the typical behaviour of the samples studied can be seen in Figure 9. The section from which Young's modulus is extracted is the linear section (initial portion) of the curve, represented by a black line in Figure 9. For each test, three samples were used, and their average values calculated, except for the blending group containing 1% of ZrO_2 NPs and the soaking group containing 0.25% of ZrO_2 NPs, in which only two samples were used instead of three due to a failure in the device.

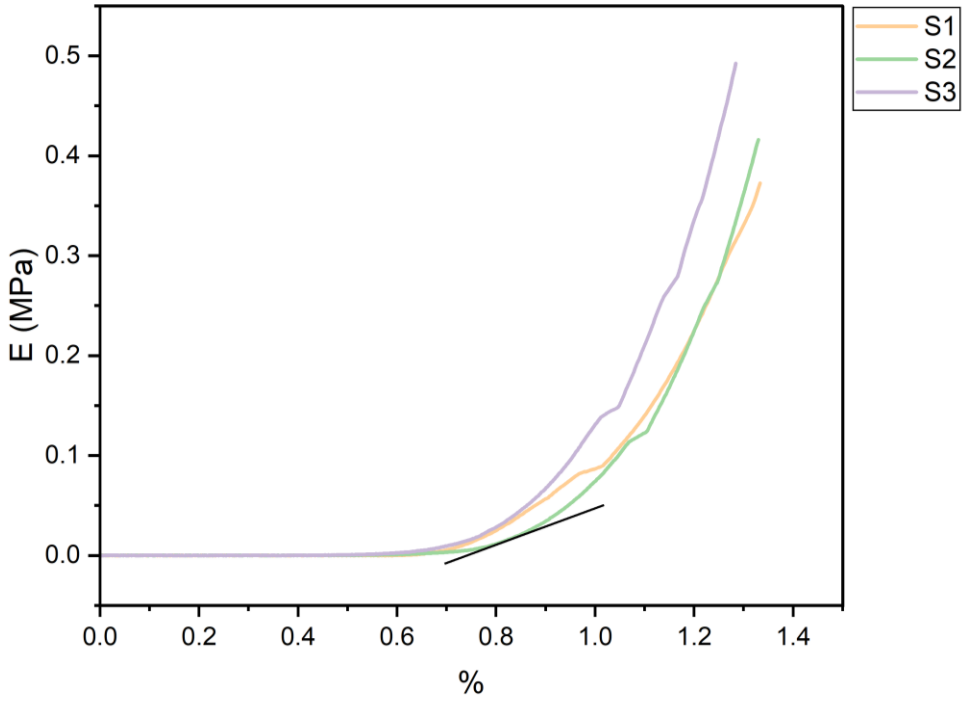

Figure 9. Representation of the mechanical behaviour of the scaffolds. The black line corresponds to the zone of the graphic where the slope was measured.

The use of nanoparticles as a reinforcement, is expected to improve the mechanical properties of the scaffold, increasing the Young's Modulus [43], [44]. However, looking at Table 2 and Figure 10 it is possible to notice that an increase of nanoparticles showed a lower elastic modulus in all the cases comparing to the control group, except when 1.5% of ZrO_2 NPs are added by the soaking method, that showed a severe increase in the Young's Modulus. Comparing both methods, the soaking one provides higher mechanical properties than the blending one, regardless the nanoparticles percentage. The elastic modulus of the soaking group increases with the increase of zirconia NPs. The same, doesn't happened with the

blending group, since 1B presents a lower Young's modulus than 025B. This behaviour might be due to the accumulation of reagents and lack of homogeneity, as we saw in Figure 5 b).

Comparing the porosity with the mechanical tests, we can verify that the groups with high values of porosity are the ones with the lowest values of Young's Modulus. Therefore, we can say that the porosity and the elastic modulus are inversely proportional. This behaviour was expected, since the architecture of the scaffold influences its mechanical behaviour, since the bigger the porosity, the lower its mechanical resistance [45]

In order for a structure to be used as an implant, the stiffness of the material should be close to or higher than the stiffness of the tissue into which it will be inserted. Unfortunately, in terms of mechanical properties, none of the scaffolds is able to mimic the mechanical properties of the osteochondral bone.

A way to improve the mechanical properties of the scaffold may be using more concentration of alginate, use more concentration of zirconia nanoparticles and do more robust alginates, increasing the height and diameter. In this conditions, the poor mechanical properties of the 3% alginate scaffold functionalized with zirconia nanoparticles would limit its application in cartilage and bone tissue engineering.

Table 2. Young's Modulus and standard deviation of the scaffolds.

	Scaffolds	Young's Modulus (MPa)
Control	ALG	0.625 ± 0.017
Blending group	0.25% of ZrO_2 NPs	0.198 ± 0.001
	1% of ZrO_2 NPs	0.165 ± 0.053
	1.5% of ZrO_2 NPs	0.388 ± 0.021
Soaking group	0.25% of ZrO_2 NPs	0.321 ± 0.017
	1% of ZrO_2 NPs	0.427 ± 0.011
	1.5% of ZrO_2 NPs	1.120 ± 0.042
Bone	Trabecular	100-2000 [47]
	Cortical	17000 [47]

Figure 10. Young's Modulus (E) obtained after compression tests on the scaffolds.

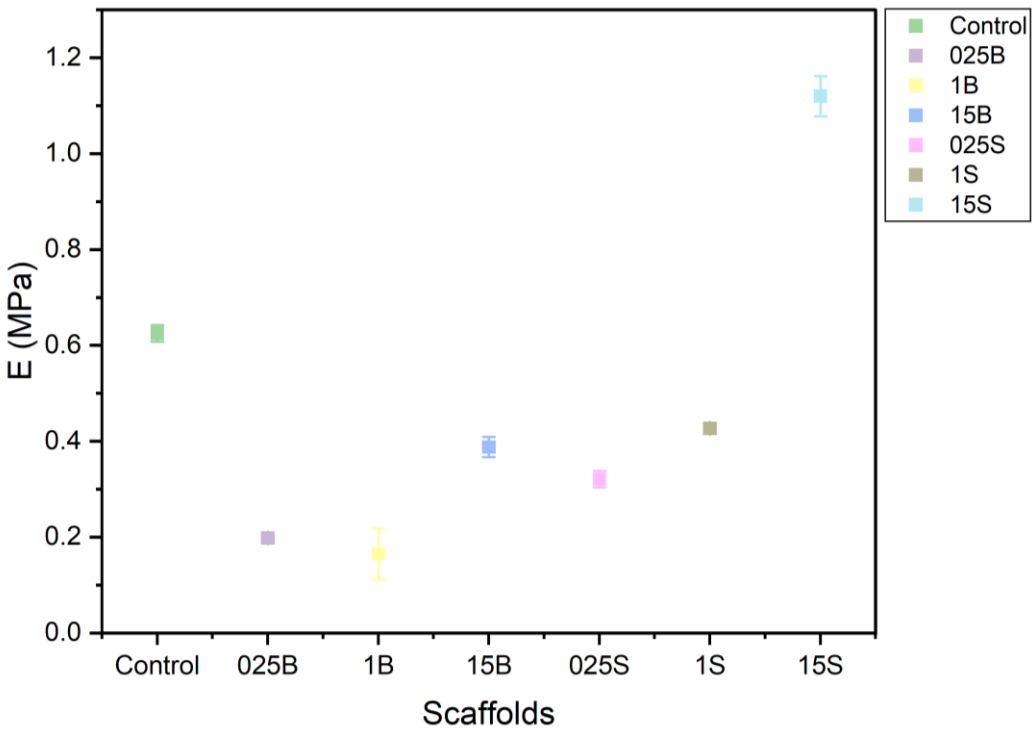

3.4 Celular Assays

The viability of the cells in the scaffolds was qualitatively assessed by the Live-Dead staining on days 1 and 7, using a fluorescent microscope. The scaffolds were sterilized and then exposed to 500 µL of culture medium. To measure how many living or death cells were present in each group, the software ImageJ were used. The images of the dead cells were overlapped on those of the live cells in order to compare the abundance of each one. Green dots represent the living cells and the red represent the dead ones. In these tests, only 025B, 1B, 025S, 1S were used. Due to the limited number of cells available, it was not possible to use the desired number of samples for each group under study. Therefore, n=1, so it is not possible to analyse the statistics of the Live-Dead assay.

Although we can notice the presence of more living cells than dead ones in Image 11, most of them are placed in the surroundings of the scaffold. This means that the scaffolds with the nanoparticles are not toxic, or else we would see a bigger quantity of red dots, but it also means that most of the cells did not adhere to the scaffold as we wanted. One way to increase the number of cells in or on top of the scaffold would be to place the medium more gently, so that the cells don't spread throughout the culture plate and remain on the scaffold.

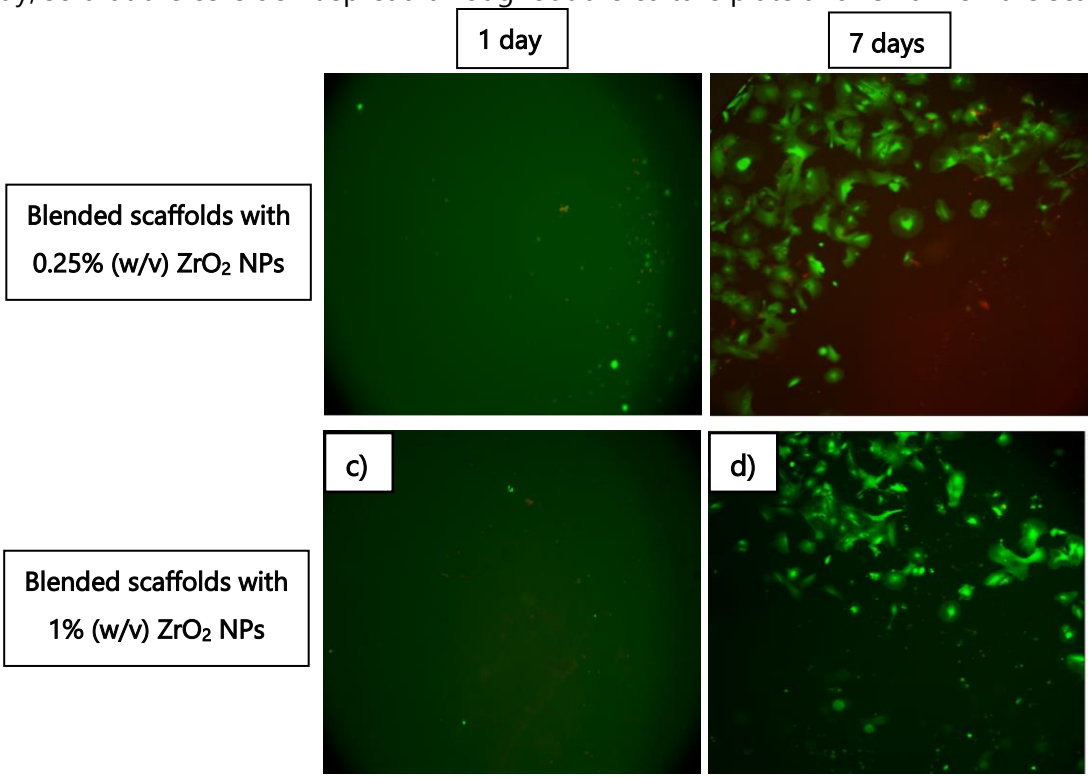

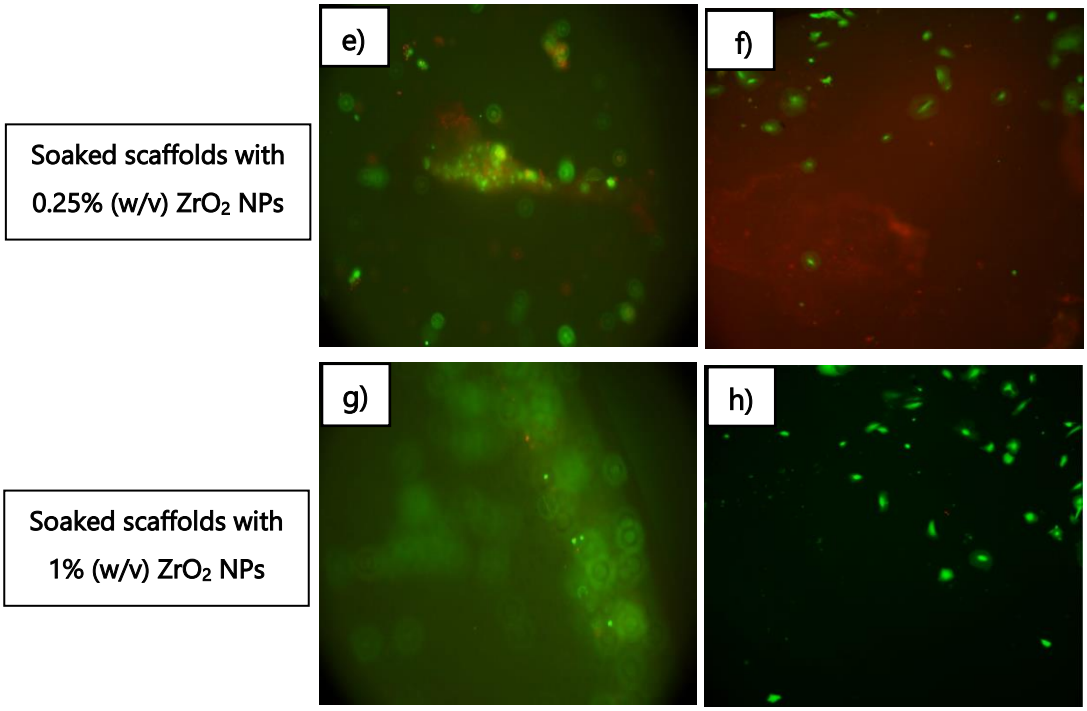

Figure 11. Live/Dead Assay performed after 1 and 7 days. Scaffolds a) blended with 0.25% NPs after 1 day. b) blended with 0.25% NPs after 7 days. c) blended with 1% NPs after 1 day. d) blended with 1% NPs after 7 days. e) soaked with 0.25% NPs after 1 day. f) soaked with 0.25% NPs after 7 days. g) soaked with 1% NPs after 1 day. h) soaked with 0.25% NPs after 7 days. The green and red dots indicate live and dead cells, respectively.

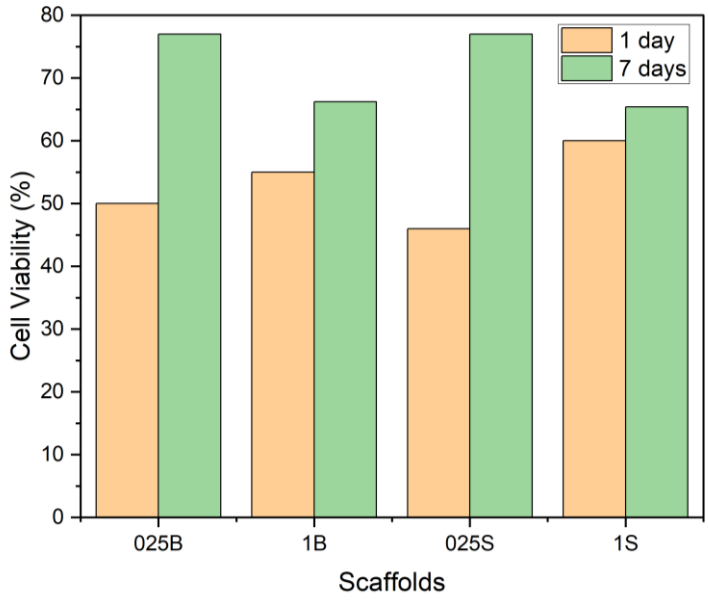

Figure 12. Graph representing the cell viability on the 4 different scaffolds.

Analysing Figure 12, we can see that the cell viability increases after 7 days, in all groups, regardless the NPs´ percentage. This means that after 7 days, more living cells tend to grow in the scaffold in its surroundings. It is also possible to conclude that the 0,25% of nanoparticles content leads to less quantity of dead cells than 1% NPs content. Also, there are no significant differences between the blending and the soaking method in cytotoxicity since the values of cell viability are very similar when compared. The groups that present the better values of cell viability were 025S and 025B, both with 77%, after 7 days. Nevertheless, live-dead assay showed that after 1 day, there are more living cells in the scaffolds containing the big amount of nanoparticles (1B and 1S) and in the scaffolds that contain 0,25% of NPs, the cell viability is less than 50%, meaning that we have more dead cells than living cells.

The results demonstrate that the scaffolds elaborated by the soaking and blending methods with 0,25% of ZrO_2 NPs do not release toxic components that could negatively impact the viability of the cells cultured on them. However, there wasn't high cell migration and penetration through the pores of the scaffolds.

4

Conclusions and future perspectives

The present work focused on the development of alginate scaffolds reinforced with different percentages of zirconia nanoparticles, by two different methods, blending and soaking technique, aiming to regenerate osteochondral tissue.

The synthesis of zirconia nanoparticles was efficiently developed, revealing agglomerations of nanospheres and a medium size of 66,19 ±7,55 nm. The obtained NPs were in the monoclinic crystalline phase, the most thermodynamically stable at room temperature. The functionalization of the scaffolds with the nanoparticles were efficiently made. Furthermore, SEM and EDS images showed that the zirconia was spread over the entire surface of the scaffold, although there were some aggregates.

The results obtained in the current study regarding the assessment of the effect of alginate scaffold functionalized with zirconia nanoparticles showed that It Is possible to obtain better porosity values with the blended scaffolds and that, by both methods, the Increase of nanoparticles causes the decrease of porosity. As for swelling, besides the control group just containing alginate, the soaked scaffolds have the best swelling rate. Since tissue engineering scaffolds with higher porosity can absorb more water, it was expected that samples made using the blending method have the highest swelling ratio. This paradoxical condition may be caused by the low amounts of nanoparticles utilized in this Investigation, which had a small effect on the swelling behavior.

Both methods showed Insufficient mechanical properties. Comparing the soaking and the blending technique, the soaking one provides higher mechanical properties than the blending one, regardless the nanoparticles percentage.

The live-dead assay showed that are a change in the cells growing after 7 days and an increase of the cell's viability after this time, which is very good. In order to draw better conclusions, it would be necessary to differentiate the cells.

Gathering this information, the soaking group with 0.25% of nanoparticles by the soaking method showed medium porosity, the best swelling rate, and the best cell viability and toxicity results. Therefore, It has the best properties for osteochondral tissue engineering.

Future work should consider optimizing the size and structure of the scaffolds. The samples used had very small dimensions, which has a very negative impact on the Young's modulus. Also, the mechanical properties could be improved using more concentration of alginate. In addition, a more concentration of zirconia NPs would help increasing the mechanical characteristics but would cause a decrease in porosity and swelling ability. The incorporation of another biomaterial such as gelatin, or even collagen, could be a good strategy to reinforce the matrix of the scaffolds, improving its similarity to osteochondral tissue.

5

REFERENCES

[1] Patcharakamon Nooeaid, "Multilayered Scaffolds for Osteochondral Tissue Engineering Based on Bioactive Glass and Biodegradable Polymers," 2014.

[2] M. Emmanuel Konstantakos, "Arthritis-health," What Is Cartilage?

[3] C. Vyas, · Hussein Mishbak, G. Cooper, C. Peach, R. F. Pereira, and P. Bartolo, "Biological perspectives and current biofabrication strategies in osteochondral tissue engineering," vol. 5, no. 2, 2020, doi: 10.1007/s40898-020-00008-y.

[4] H. H. M. Mishbak, P. J. Bartolo, and G. Cooper, "Design and fabrication of scaffolds for cartilage applications through photopolymerization of hydrogels School of Mechanical, Aerospace and Civil Engineering," University of Manchester, 2019.

[5] F. Horkay, "Interactions of Cartilage Extracellular Matrix Macromolecules," 2012, doi: 10.1002/polb.23191.

[6] L. Zhang, J. Hu, and K. A. Athanasiou, "The Role of Tissue Engineering in Articular Cartilage Repair and Regeneration," *Crit Rev Biomed Eng*, vol. 37(1–2), 2009.

[7] G. Li *et al.*, "Subchondral bone in osteoarthritis: insight into risk factors and microstructural changes." [Online]. Available: http://arthritis-research.com/content/15/6/223

[8] X. Hu *et al.*, "Therapeutic 'Tool' in Reconstruction and Regeneration of Tissue Engineering for Osteochondral Repair," *Applied Biochemistry and Biotechnology*, vol. 191, no. 2. Springer, pp. 785–809, Jun. 01, 2020. doi: 10.1007/s12010-019-03214-8.

[9] L. Roseti and B. Grigolo, "Current concepts and perspectives for articular cartilage regeneration," *Journal of Experimental Orthopaedics*, vol. 9, no. 1. Springer Science and Business Media Deutschland GmbH, Dec. 01, 2022. doi: 10.1186/s40634-022-00498-4.

[10] "A National Public Health Agenda for Osteoarthritis 2020."

[11] C. Juneau, R. Paine, E. Chicas, E. Gardner, L. Bailey, and J. McDermott, "CURRENT CONCEPTS IN TREATMENT OF PATELLOFEMORAL OSTEOCHONDRITIS DISSECANS," 2016.

[12] R. Hayser, MD, D. R., Steilen-Matias, MMS, and PA-C, "Non-surgical treatments for Osteochondritis dissecans." Accessed: Jun. 22, 2023. [Online]. Available: caringmedical.com/prolotherapy-news/osteochondritis-dissecans/

[13] M. Chimutengwende-Gordon, J. Donaldson, and G. Bentley, "Current solutions for the treatment of chronic articular cartilage defects in the knee," *EFORT Open Rev*, vol. 5, no. 3, pp. 156–163, Mar. 2020, doi: 10.1302/2058-5241.5.190031.

[14] M. Howell, Q. Liao, and C. W. Gee, "Surgical Management of Osteochondral Defects of the Knee: An Educational Review", doi: 10.1007/s12178-020-09685-1/Published.

[15] W. Wei and H. Dai, "Articular cartilage and osteochondral tissue engineering techniques: Recent advances and challenges," *Bioactive Materials*, vol. 6, no. 12. KeAi Communications Co., pp. 4830–4855, Dec. 01, 2021. doi: 10.1016/j.bioactmat.2021.05.011.

[16] J. Aragón and F. Zaragoza, "Nanofibrous Membranes Obtained by Electrospinning for Bone Tissue Engineering and Wound Dressing Applications," 2019.

[17] I. Gadjanski and G. Vunjak-Novakovic, "Challenges in engineering osteochondral tissue grafts with hierarchical structures Ivana Gadjanski, Gordana Vunjak Novakovic", doi: 10.1517/14712598.2015.1070825.

[18] H. Madry, J. K. Venkatesan, N. Carballo-pedrares, A. Rey-rico, and M. Cucchiarini, "Scaffold-mediated gene delivery for osteochondral repair," *Pharmaceutics*, vol. 12, no. 10. MDPI AG, pp. 1–23, Oct. 01, 2020. doi: 10.3390/pharmaceutics12100930.

[19] R. Tonndorf, D. Aibibu, and C. Cherif, "Molecular Sciences Isotropic and Anisotropic Scaffolds for Tissue Engineering: Collagen, Conventional, and Textile Fabrication Technologies and Properties," 2021, doi: 10.3390/ijms22179561.

[20] S. E. Doyle *et al.*, "3D printed multiphasic scaffolds for osteochondral repair: Challenges and opportunities," *International Journal of Molecular Sciences*, vol. 22, no. 22. MDPI, Nov. 01, 2021. doi: 10.3390/ijms222212420.

[21] J. Sun and H. Tan, "Alginate-based biomaterials for regenerative medicine applications," *Materials*, vol. 6, no. 4. pp. 1285–1309, 2013. doi: 10.3390/ma6041285.

[22] R. Abka-khajouei, L. Tounsi, N. Shahabi, A. K. Patel, S. Abdelkafi, and P. Michaud, "Structures, Properties and Applications of Alginates," *Marine Drugs*, vol. 20, no. 6. MDPI, Jun. 01, 2022. doi: 10.3390/md20060364.

[23] O. D. Frent *et al.*, "Sodium Alginate—Natural Microencapsulation Material of Polymeric Microparticles," *International Journal of Molecular Sciences 2022, Vol. 23, Page 12108*, vol. 23, no. 20, p. 12108, Oct. 2022, doi: 10.3390/IJMS232012108.

[24] M. L. Matias *et al.*, "A Comparison between Solution-Based Synthesis Methods of ZrO2 Nanomaterials for Energy Storage Applications," *Energies (Basel)*, vol. 15, no. 17, Sep. 2022, doi: 10.3390/en15176452.

[25] A. Bumajdad, A. A. Nazeer, F. Al Sagheer, S. Nahar, and M. I. Zaki, "Controlled Synthesis of ZrO2 Nanoparticles with Tailored Size, Morphology and Crystal Phases via Organic/Inorganic Hybrid Films," *Sci Rep*, vol. 8, no. 1, Dec. 2018, doi: 10.1038/s41598-018-22088-0.

[26] G. Yang and S. J. Park, "Conventional and microwave hydrothermal synthesis and application of functional materials: A review," *Materials*, vol. 12, no. 7. MDPI AG, 2019. doi: 10.3390/ma12071177.

[27] H. V Almeida, B. N. Sathy, I. Dudurych, C. T. Buckley, F. J. O'brien, and D. J. Kelly, "Anisotropic Shape-Memory Alginate Scaffolds Functionalized with either Type I or Type II Collagen for Cartilage Tissue Engineering," 2017.

[28] Y. Zhao *et al.*, "Use of silver nanoparticle–gelatin/alginate scaffold to repair skull defects," *Coatings*, vol. 10, no. 10, pp. 1–12, Oct. 2020, doi: 10.3390/coatings10100948.

[29] X. Zhang *et al.*, "Doubly crosslinked biodegradable hydrogels based on gellan gum and chitosan for drug delivery and wound dressing," *Int J Biol Macromol*, vol. 164, pp. 2204–2214, Dec. 2020, doi: 10.1016/j.ijbiomac.2020.08.093.

[30] S. Ding, J. Zhao, and Q. Yu, "Effect of Zirconia Polymorph on Vapor-Phase Ketonization of Propionic Acid," 2019, doi: 10.3390/catal9090768.

[31] J. Lombardi *et al.*, "Direct Observation of Enhanced Raman Scattering on Nano-Sized ZrO 2 Substrate: Charge-Transfer Contribution," *Front. Chem*, vol. 7, p. 245, 2019, doi: 10.3389/fchem.2019.00245.

[32] S. N. Basahel, T. T. Ali, M. Mokhtar, and K. Narasimharao, "Influence of crystal structure of nanosized ZrO2 on photocatalytic degradation of methyl orange," *Nanoscale Res Lett*, vol. 10, no. 1, 2015, doi: 10.1186/s11671-015-0780-z.

[33] A. Bumajdad, A. A. Nazeer, F. Al Sagheer, S. Nahar, and M. I. Zaki, "Controlled Synthesis of ZrO2 Nanoparticles with Tailored Size, Morphology and Crystal Phases via Organic/Inorganic Hybrid Films," *Sci Rep*, vol. 8, no. 1, Dec. 2018, doi: 10.1038/s41598-018-22088-0.

[34] M. Bahraminasab, "Challenges on optimization of 3D-printed bone scaffolds," *BioMedical Engineering Online*, vol. 19, no. 1. BioMed Central Ltd, Sep. 03, 2020. doi: 10.1186/s12938-020-00810-2.

[35] C. M. Murphy and F. J. O'Brien, "Understanding the effect of mean pore size on cell activity in collagen-glycosaminoglycan scaffolds," *Cell Adhesion and Migration*, vol. 4, no. 3. Taylor and Francis Inc., pp. 377–381, 2010. doi: 10.4161/cam.4.3.11747.

[36] J. Folgado and P. R. Fernandes, "Bone Tissue Mechanics PART 4 and 5".

[37] F. Abedi, S. V. Moghaddam, P. Ghandforoushan, M. Aghazadeh, H. Ebadi, and S. Davaran, "Synthesis and characterization of growth factor free nanoengineered bioactive scaffolds for bone tissue engineering," *J Biol Eng*, vol. 16, no. 1, Dec. 2022, doi: 10.1186/s13036-022-00303-x.

[38] N. Asadi, E. Alizadeh, A. Rahmani Del Bakhshayesh, E. Mostafavi, A. Akbarzadeh, and S. Davaran, "Fabrication and in Vitro Evaluation of Nanocomposite Hydrogel Scaffolds Based on Gelatin/PCL-PEG-PCL for Cartilage Tissue Engineering," *ACS Omega*, vol. 4, no. 1, pp. 449–457, Jan. 2019, doi: 10.1021/acsomega.8b02593.

[39] K. Aranci *et al.*, "3D Propolis-Sodium Alginate Scaffolds: Influence on Structural Parameters, Release Mechanisms, Cell Cytotoxicity and Antibacterial Activity," *Molecules*, vol. 25, no. 21, Nov. 2020, doi: 10.3390/molecules25215082.

[40] C. Gao, M. Liu, J. Chen, and X. Zhang, "Preparation and controlled degradation of oxidized sodium alginate hydrogel," *Polym Degrad Stab*, vol. 94, no. 9, pp. 1405–1410, Sep. 2009, doi: 10.1016/j.polymdegradstab.2009.05.011.

[41] J. Su, H. Xu, J. Sun, X. Gong, and H. Zhao, "Dual delivery of BMP-2 and bFGF from a new nano-composite scaffold, loaded with vascular stents for large-size mandibular defect regeneration," *Int J Mol Sci*, vol. 14, no. 6, pp. 12714–12728, 2013, doi: 10.3390/ijms140612714.

[42] X. Hao *et al.*, "Angiogenic effects of sequential release of VEGF-A165 and PDGF-BB with alginate hydrogels after myocardial infarction," *Cardiovasc Res*, vol. 75, no. 1, pp. 178–185, Jul. 2007, doi: 10.1016/j.cardiores.2007.03.028.

[43] M. Ghanbari, M. Salavati-Niasari, F. Mohandes, Z. Firouzi, and S. D. Mousavi, "The impact of zirconium oxide nanoparticles content on alginate dialdehyde-gelatin scaffolds in cartilage tissue engineering," *J Mol Liq*, vol. 335, Aug. 2021, doi: 10.1016/j.molliq.2021.116531.

[44] B. Nasri-Nasrabadi *et al.*, "Sodium alginate/magnesium oxide nanocomposite scaffolds for bone tissue engineering," *Polym Adv Technol*, vol. 29, no. 9, pp. 2553–2559, Sep. 2018, doi: 10.1002/pat.4367.

[45] Bianca Catarina Guimarães da Silva, "Fabrico de scaffolds porosos de vidro bioativo para regeneração óssea," 2015.

A
AN APPENDIX

A.1 Alginate Solution

As mentioned before, using a previous report from Henrique Vazão de Almeida Phd., the alginate solution was produced. Firstly, 0,1M of MES (2-(N-Morpholino) ethanesulfonic acid buffer, Sigma-Aldrich, CAS: 71119-23-8, C6H13NO4S) and 0,2M of NaCl (Sigma-Aldrich, CAS: 7647-14-5) was mixed in 5 mL of distilled water. 3,3% w/v of Sodium Alginate (Sigma-Aldrich, CAS: 9005-38-3) was added and dissolved in the previous solution. Solutions of N-Hydroxysuccinimide (Sigma-Aldrich, CAS:6066-62-6; NHS) and 1-ethyl-3-3dimethyl aminopropyl carbodiimide (Sigma-Aldrich, CAS: 1892-57-5; EDAC) were homogenized with alginate solution (5 minutes) with a final molar ratio of 2:1:2 for EDAC:NHS:COO-. Additionally, adipic acid dihydrazide (Sigma-Aldrich, CAS: 1071-93-8; AAD) was added to promote the crosslinking in a ratio of 45% compared to alginate. The solution was transferred to a Petri dish and gelified overnight. The obtained hydrogel was washed with water and 0.1M of CaCl2 to remove chemical agents several times. The hydrogel was cutted in small pieces.

A.2 Nanoparticles measurements

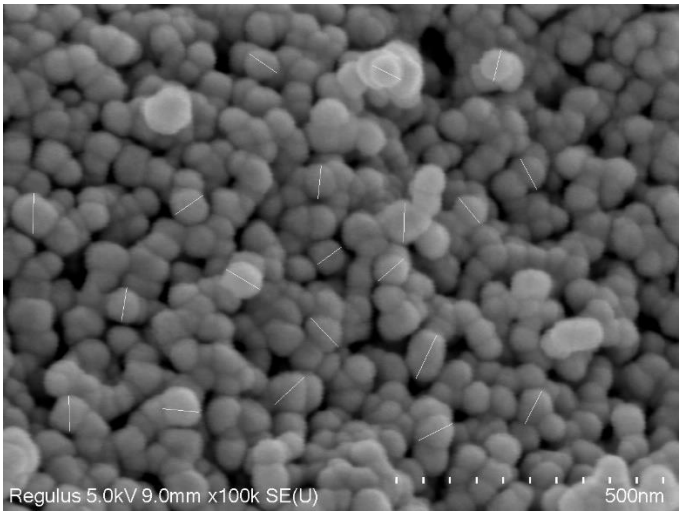

Figure 13. Measures of different nanoparticles from Figure 3.

Results

File Edit Font Results

	Area	Mean	StdDev	Min	Max	Angle	Length
1	71.385	148.276	8.438	113	161.997	-30.700	72.615
2	60.916	118.310	14.906	80	142.816	34.695	61.703
3	73.289	120.341	17.678	77	156.000	88.493	74.172
4	65.675	137.654	8.233	115	153.324	-5.042	66.599
5	56.157	168.757	10.730	153.578	191.018	-26.565	56.720
6	73.289	105.194	25.985	60.000	144.371	42.879	74.556
7	85.663	111.223	24.332	52.000	163.000	64.592	86.406
8	52.349	86.318	11.282	34.000	96.556	36.027	53.079
9	69.482	121.713	23.045	76.519	157.272	26.565	69.809
10	71.385	130.818	7.678	115.000	148.378	88.452	72.221
11	60.916	120.717	7.363	88.250	128.000	129.864	61.645
12	59.964	105.282	22.318	46.000	136.290	84.472	60.770
13	60.916	119.266	12.029	90.000	136.000	-34.695	61.703
14	63.771	119.118	16.345	73.000	143.000	91.736	64.420
15	61.867	91.733	13.065	43.000	104.348	118.361	62.640
16	72.337	110.001	8.537	74.000	119.201	133.919	73.138
17	61.867	128.561	26.410	65.000	170.750	41.186	62.225
18	67.578	107.487	23.930	67.511	145.675	62.700	68.069
19	62.819	114.099	18.186	64.000	136.663	81.119	63.196
20	58.060	153.022	8.567	122.000	170.942	-103.570	58.210

Figure 14. Measures and mean value of Figure 3.

A.3 Diffractograms of Zr02 crystalline phases

Monoclinic phase (ICDD 00-036-0420)

Date: 24-06-2022 Time: 16: File: HighScore Plus - ZrO2_230C_25min_Anealling800C15min User: Administrator

Name and formula

Reference code:	00-036-0420
Mineral name:	Baddeleyite, syn
Compound name:	Zirconium Oxide
PDF index name:	Zirconium Oxide
Empirical formula:	O_2Zr
Chemical formula:	ZrO_2

Crystallographic parameters

Crystal system:	Monoclinic
Space group:	P21/c
Space group number:	14
a (Å):	5.1463
b (Å):	5.2135
c (Å):	5.3110
Alpha (°):	90.0000
Beta (°):	99.2000
Gamma (°):	90.0000
Calculated density (g/cm^3):	5.82
Measured density (g/cm^3):	5.71
Volume of cell (10^6 pm^3):	140.66
Z:	4.00
RIR:	2.60

Status, subfiles and quality

Status:	Marked as deleted by ICDD
Subfiles:	Alloy, metal or intermetalic, Forensic, Inorganic, Mineral
Quality:	Star (S)

Comments

Color:	White
Color:	White
Sample Preparation:	Reagent grade ZrO_2 fired at 1250 C for 72 hours then cooled in air
Additional Patterns:	To replace 13-307. Validated by calculated pattern 24-1165
Optical Data:	A=2.13, B=2.19, Q=2.20, Sign=-, 2V=30°*. Pattern reviewed by Holzer, J., McCarthy, G., North Dakota State University, Fargo, North Dakota, USA, JCPDS Grant-in-Aid Report (1990). Agrees well with experimental and calculated patterns. Additional weak reflection [indicated by bracket] was observed
Deleted Or Rejected By:	Deleted by 37-1484, lower F_N, MTG 5/92.

References

Primary reference: Larson, F., McCarthy, G., North Dakota State University, Fargo, North Dakota, USA., ICDD Grant-in-Aid, (1985)

Peak list

No.	h	k	l	d [Å]	2θ [°]	I [%]
1	1	0	0	5.07900	17.447	6.0
2	0	1	1	3.69400	24.072	18.0
3	-1	1	0	3.63600	24.462	12.0
4	-1	1	1	3.16300	28.190	100.0
5	1	1	1	2.83900	31.487	64.0
6	0	0	2	2.62000	34.196	22.0
7	0	2	0	2.60500	34.399	12.0
8	2	0	0	2.54000	35.308	14.0
9	-1	0	2	2.49700	35.936	3.0
10	0	1	2	2.34200	38.405	1.0
11	0	2	1	2.33200	38.576	5.0
12	-2	1	0	2.28300	39.438	1.0

13	-1	1	2	2.25300	39.985	1.0
14	-2	1	1	2.21310	40.738	12.0
15	1	0	2	2.19050	41.177	6.0
16	-1	2	1	2.18000	41.384	5.0
17	1	1	2	2.01910	44.854	7.0
18	2	1	1	1.99100	45.522	6.0
19	-2	1	2	1.85930	48.950	3.0
20	0	2	2	1.84800	49.269	16.0
21	-2	2	0	1.81860	50.120	18.0
22	-1	2	2	1.80320	50.578	12.0
23	-2	2	1	1.78250	51.208	4.0
24	2	0	2	1.69340	54.115	11.0
25	1	2	2	1.67680	54.695	1.0
26	2	2	1	1.66030	55.285	8.0
27	0	1	3	1.65670	55.415	12.0
28	-1	1	3	1.65080	55.630	10.0
29	0	3	1	1.64830	55.722	5.0
30	-1	3	0	1.64340	55.903	7.0
31	2	1	2	1.61040	57.152	7.0
32	-1	3	1	1.59160	57.891	4.0
33	-2	2	2	1.58190	58.280	4.0
34	1	3	1	1.54550	59.790	8.0
35	-3	0	2	1.53920	60.060	8.0
36	1	1	3	1.50880	61.399	6.0
37	-2	1	3	1.49560	62.001	7.0
38	3	1	1	1.47690	62.875	8.0
39	0	2	3	1.45140	64.109	2.0
40	0	3	2	1.44740	64.308	3.0
41	-2	3	0	1.43360	65.002	1.0
42	-1	3	2	1.42600	65.392	3.0
43	2	2	2	1.41970	65.719	7.0
44	-2	3	1	1.41580	65.923	4.0
45	1	3	2	1.36100	68.941	2.0
46	1	2	3	1.34870	69.660	1.0

Stick Pattern

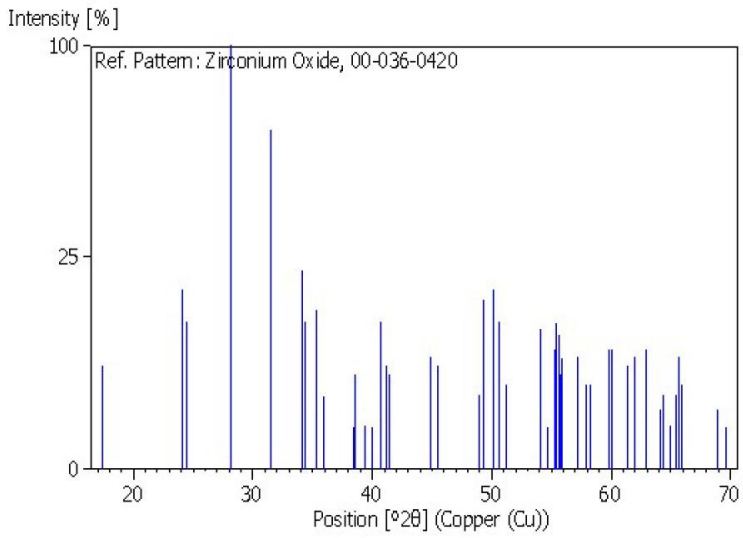

Tetragonal phase (ICDD 00-050-1089)

Date: 24-06-2022 Time: 16: File: HighScore Plus - ZrO2_230C_25min_Anealling800C15min User: Administrator

Name and formula

Reference code:	00-050-1089
Compound name:	Zirconium Oxide
PDF index name:	Zirconium Oxide
Empirical formula:	O_2Zr
Chemical formula:	ZrO_2

Crystallographic parameters

Crystal system:	Tetragonal
Space group:	P42/nmc
Space group number:	137
a (Å):	3.5984
b (Å):	3.5984
c (Å):	5.1520
Alpha (°):	90.0000
Beta (°):	90.0000
Gamma (°):	90.0000
Calculated density (g/cm^3):	-1.00
Measured density (g/cm^3):	-1.00
Volume of cell (10^6 pm^3):	66.71
Z:	2.00
RIR::	-

Subfiles and quality

Subfiles:	Alloy, metal or intermetallic, Ceramic, Corrosion, Inorganic
Quality:	Star (S)

Comments

t-Phase. Sample Preparation: An ammonia solution was added to a solution of $ZrOCl_2$ to form a gel. The partially dried gel was slowly heated to 600 C under nitrogen, then quenched to room temperature. Tetragonal phase is stable between 1170 C and 2370 C. Pattern taken on metastable phase at room temperature

Additional Patterns: See ICSD 85322 (PDF 88-1007).

References

Primary reference: Malek, J., Benes, L., Mitsuhashi, T., Powder Diffraction, **12**, 96, (1997)

Peak list

No.	h	k	l	d [Å]	2θ [°]	I [%]
1	0	1	1	2.95020	30.271	100.0
2	0	0	2	2.57504	34.812	8.0
3	1	1	0	2.54361	35.256	12.0
4	0	1	2	2.09529	43.140	1.0
5	1	1	2	1.80989	50.378	43.0
6	0	2	0	1.79875	50.712	22.0
7	0	1	3	1.54970	59.612	14.0
8	1	2	1	1.53580	60.207	24.0
9	2	0	2	1.47491	62.969	7.0
10	0	0	4	1.28793	73.467	3.0
11	2	2	0	1.27202	74.540	5.0
12	1	2	3	1.17444	81.974	11.0
13	0	3	1	1.16854	82.477	6.0
14	1	1	4	1.14899	84.198	4.0
15	2	2	2	1.14106	84.920	3.0
16	1	3	0	1.13774	85.226	3.0
17	0	2	4	1.04715	94.718	3.0
18	1	3	2	1.04080	95.480	9.0

Date: 24-06-2022 Time: 16: File: HighScore Plus - ZrO2_230C_25min_Anealling800C15min User: Administrator

Stick Pattern

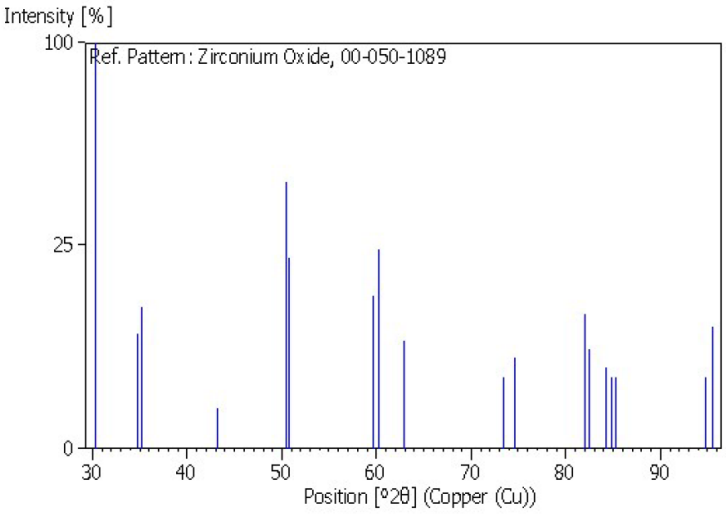

Cubic phase (ICDD 00-051-1149)

Date: 24-06-2022 Time: 16: File: HighScore Plus - ZrO2_230C_25min_Anealling800C15min User: Administrator

Name and formula

Reference code:	00-051-1149
Compound name:	Zirconium Oxide
PDF index name:	Zirconium Oxide
Empirical formula:	OZr
Chemical formula:	ZrO

Crystallographic parameters

Crystal system:	Cubic
Space group:	Fm-3m
Space group number:	225
a (Å):	4.6258
b (Å):	4.6258
c (Å):	4.6258
Alpha (°):	90.0000
Beta (°):	90.0000
Gamma (°):	90.0000
Calculated density (g/cm^3):	-1.00
Measured density (g/cm^3):	-1.00
Volume of cell (10^6 pm^3):	98.98
Z:	4.00
RIR::	-

Subfiles and quality

Subfiles:	Alloy, metal or intermetalic, Corrosion, Inorganic

Quality: Star (S)

Comments

Sample Preparation: A mixture of 20 wt.% Al and ZrO_2 was heated to 1500 C and held for 0.5 hours under 7 MPa pressure

Additional Patterns: See 20-684 for calculated intensities and d-values.

References

Primary reference: Zhe, X., Hendry, A., J. Mater. Sci. Lett., **17**, 687, (1998)

Peak list

No.	h	k	l	d [Å]	2θ [°]	I [%]
1	1	1	1	2.67050	33.530	100.0
2	2	0	0	2.31310	38.904	91.0
3	2	2	0	1.63500	56.215	48.0
4	3	1	1	1.39450	67.061	35.0
5	2	2	2	1.33530	70.462	13.0
6	4	0	0	1.15650	83.527	9.0
7	3	3	1	1.06110	93.095	12.0
8	4	2	0	1.03420	96.288	18.0
9	4	2	2	0.94440	109.303	14.0

Stick Pattern

Date: 24-06-2022 Time: 16: File: HighScore Plus - ZrO2_230C_25min_Anealling800C15min User: Administrator